Laser Doppler Velocimeter Measurement in the Tip Region of a Compressor Rotor

K.N.S. Murthy* and B. Lakshminarayana†
The Pennsylvania State University, University Park, Pennsylvania

The axial and tangential velocity components near the tip region of a compressor rotor were measured using a laser Doppler velocimeter. The measurements were taken at 25 radial locations in the outer 20% of the blade span and at 10 axial locations upstream, inside, and at the exit of the rotor. The result are interpreted to derive the behavior of the leakage flow and the inviscid effects. The inviscid and annulus-wall boundary-layer effects dominated up to one-quarter-chord position, beyond which the leakage phenomena had a major influence in altering the flow characteristics in the outer 10% of the blade span. The velocity field measured near the leading edge revealed the effects of rapid acceleration near the suction surface and the influence of the stagnation point on the pressure surface.

Nomenclature

C_R	= axial chordlength at the tip, 10.9 cm
p	= static pressure
PS	= pressure surface
R	= nondimensional radius, $= r/r_t$
r,θ,z	= radial, tangential, and axial coordinates, respectively
S	= blade spacing
SS	= suction surface
T_x, T_θ	= turbulence intensities in axial and tangential directions, respectively
t	= tip clearance heights
U	= blade speed
V_z, V_θ, V_r	= axial, tangential, and radial velocity components of absolute flow normalized by blade tip speed; 53 m/s
W_x, W_θ	= axial and tangential relative velocity components normalized by blade tip speed; 53 m/s
X_R	= distance from the rotor leading edge normalized by C_R ($X_R = 0.0$ and 1.0 correspond to the leading and trailing edges, respectively)
Y	= tangential distance measured from suction surface normalized by local blade spacing ($= r\theta/S$, $\theta = 0$ on the suction surface)
ρ	= fluid density
Subscripts	
h,t	= hub and tip, respectively
w	= wall
Superscript	
$(\ )'$	= passage averaged

Introduction

THE flowfield in the tip region is one of the least understood phenomenon in a turbomachinery rotor. The flowfield at the rotor blade tip reduces efficiency and reliability and introduces off-design conditions in downstream stages. Thus, a good understanding of the nature of the flowfield at the rotor blade tip should lead to techniques that would improve turbomachinery performance.

The development of computational techniques for the rotor flows is a formidable task, involving modeling of several features of the turbulent flow. The development of computational techniques to predict the end-wall flowfield requires an accurate set of data for validation. Hence, the objective of the present investigation is to provide an accurate set of data, using a nonintrusive technique, for the use of computors.

Earlier attempts to investigate the flowfield in the tip region have been based mainly on intrusive measurement techniques, such as three-sensor hot-wire[1] and flow-visualization[2] techniques used in compressor rotors.

The laser Doppler velocimeter (LDV) is the most suitable choice for a nonstationary flowfield measurement. The earliest use of the LDV system in the turbomachinery field was in the early 1970s. The early investigators had to resort to either slow camera recording and sampling techniques[3] or gating of the data acquisition system[4]; these techniques, however, tend to be inefficient and time-consuming. The motion-camera recording cannot be adopted for rapid and efficient data acquisition. Powell et al.[5] and Strazisar and Powell[6] considerably improved the data acquisition process, and developed an efficient method for turbomachinery applications.

The objective of this paper is to report the mean flow measurement in the end-wall region of a compressor rotor using a procedure similar to that in Ref. 6. None of the previous investigators have acquired detailed data in the end-wall region using the LDV.

Experimental Facility and Program

The end-wall flow measurements were carried out in a single-stage axial flow compressor facility in the Department of Aerospace Engineering of The Pennsylvania State University. Overall performance of the facility is presented in Ref. 7. Good peak efficiencies are exhibited by the rotor. The hub/annulus wall diameter ratio of the facility is 0.5, with the diameter of the annulus wall equal to 0.9377 m. The inlet guide vane (IGV) row, consisting of 43 blades, is followed by a 21-bladed rotor. The rotor is driven by a 37-kW variable-speed motor, followed by a stator row of 25 blades. Downstream of the stator, an axial flow fan, with a variable

Presented as Paper 84-1602 at the AIAA 17th Fluid Dynamics, Plasma Dynamics, and Lasers Conference, Snowmass, CO, June 25-27, 1984; received July 9, 1984; revision received Oct. 1, 1985.

*Graduate Assistant.

†Distinguished Alumni Professor of Aerospace Engineering and Director of Computational Fluid Dynamic Studies. Fellow AIAA.

blade setting, is used to control the pressure rise and mass flow through the facility.

Operating conditions and rotor specifications are: inlet velocity, $V_{z\infty}$, 29.5 m/s; flow coefficient based on a tip speed of 0.56; stage loading coefficient based on a tip speed of 0.4864; rotor speed, 1080 rpm; and tip clearance, 2.5-3.0 mm. The blade section at the rotor blade tip corresponds to an NACA 65 series, where the chordlength is 15.41 cm spacing, 14.12 cm, maximum thickness, 5.10% of chord; stagger angle, 45.0 deg; and maximum camber height, 8% of chord. The blade element data for the rotor and IGV are given in Table V of Ref. 7.

The LDV measurements were taken at 10 axial locations, i.e., $X_R = 0$, 0.25, 0.5, 0.75, 1.0, 1.04, 1.17, 1.41, 2.0, 3.0. The velocity data at the rotor inlet ($X_R = -0.35$), acquired with a conventional probe, is shown in Fig. 1.

At each axial location, nearly 25 radial surveys were conducted to map the velocity distribution inside the rotor passage. The radial station nearest the casing wall was at $R = 0.98$ (very close to the blade tip and 5 mm from the wall), and the one farthest from the casing wall was at $R = 0.902$.

A quartz window of 25.4 mm diameter and 6.35 mm thickness was used to transmit the laser beams into the rotor passage. The quartz window was mounted on a plexiglass cover which was formed to match the inner contour of the outer casing. The quartz window was also coated with an antireflective coating that helped reduce the glare from the wall. In addition, the rotor was coated with an orange fluorescent enamel, Deristo C-GLO 913 Red. During the experimental investigation, the rotor intercepted the laser beam and scattered an orange light. The scattered light collected by the receiving optics was comprised of the real signal, green in color, which was scattered by the seed particle, and the noise, orange in color, was scattered by the rotor. An orange filter was used on the orange background noise before directing the scattered light onto the photomultiplier tube. The orange filter had a peak transmittance of 80% at a central wavelength of 514.5 mm and a half-bandwidth of 6.4 mm. This procedure helped to reduce the background noise drastically.

The nearest radial station investigated was 5 mm from the casing wall. Since the probe volume length was 2.03 mm, there was not enough spatial resolution to probe the flow inside the clearance region. In addition, the flowfield in the clearance region could not be measured due to interference caused by the wall reflection.

The flow was seeded with a 0.6-2 μm atomized spray of mineral oil, and was injected into the flow upstream of the rotor.

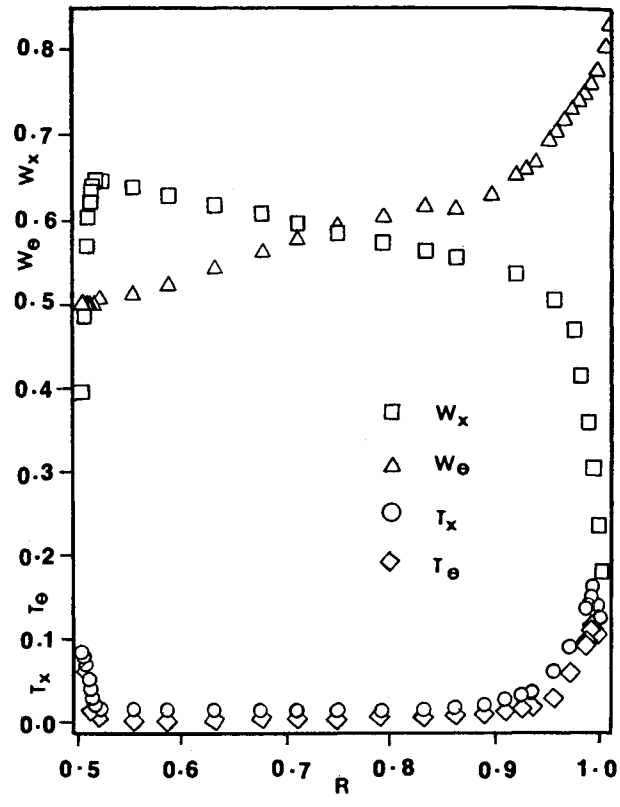

Fig. 1 Inlet axial and tangential velocity profiles and turbulent intensities at $X_R = -0.35$.

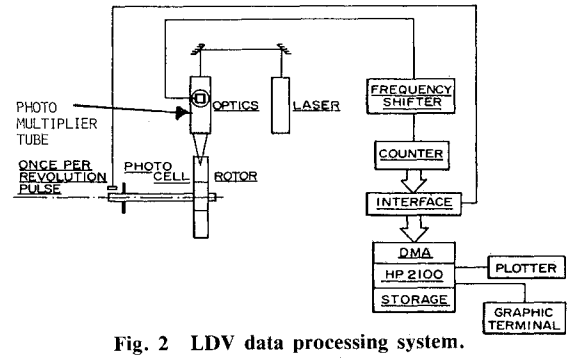

Fig. 2 LDV data processing system.

LDV System, Data Reduction, Processing, and Error Estimates

A single-channel, fringe-type laser Doppler velocimeter, with on-axis backscatter light collection (TSI model 9100-6) was used for the measurement. The system operated with a 4-W Lexel argon-ion laser tuned for the green color (514.5 mm). The entire system, comprised of the laser and the transmitting and receiving optics, was mounted on an x-y-z traversing table. The table could be moved both along and perpendicular to the optical axis, with a facility to tilt the table in the vertical plane. The entire assembly was mounted on a hydraulically controlled bench capable of moving in the vertical direction. The three linear degrees of freedom, with the possibility of tilting the table, enabled the bisector of the beam to be positioned accurately in the radial direction.

Only one component of the velocity lying in the plane of the beam, but perpendicular to the bisectors of the beam, could be measured with a single-channel LDV. Hence, the measurement of either the tangential or axial velocity component was made by rotating the plane of the beam. This was achieved by rotating the beamsplitter. The ability to position the beam bisector in an off-radial direction should, in principle, help in measuring the radial component of velocity; however, this was not attempted.

The transmitting optics consisted of a beamsplitter, a 3.75× beam expander, and a 152-mm-diam front lens with a focal length of 762 mm. The half-angle of the intersecting beam was 3.12 deg, and provided a probe volume diameter and length of 0.111 and 2.03 mm, respectively, based on the $1/e^2$ intensity points. If necessary (as in the case of the directional ambiguity, the pedestal removal, or the frequency compression), one of the split beams could be shifted in frequency with respect ot the other. This was achieved by passing one of the beams through the Bragg cell energized at 40 MHz. The optical wedges were used in the Bragg cell to correct the beam deflection.

The scattered light from the particles passing the probe volume was received by a 152-mm-diam lens, and was directed to the photomultiplier through a field stop unit and a receiving assembly. The field stop consisted of a focusing lens, an aperture of 0.008 in. in diameter, and a filter. A

beamsplitter was used to orient the fringe pattern at 90 deg in a plane perpendicular to the compressor axis.

Data Processing Procedure

In order to process an enormous amount of data generated at a rapid rate, a counter-type signal processor, interfaced with a HP 2100S computer, was used. Figure 2 shows the data processing system with direct memory access to the computer.

The signal from the photomultiplier tube was fed into the counter, wherein the signal was filtered to remove the pedestal. The period for eight cycles of the Doppler burst was measured with a resolution of 1 ns. The signal was validated and digitized. During the validation, the time for N cycles and twice the $N/2$ cycles was measured. If both agreed within the selected percentage, the data was accepted as a valid signal. The digitized data consisted of 16 bits; 12 for the mantissa and 4 for the exponent. An interface helped in direct transfer of data generated by the signal processor via direct memory access. The processor also logged the time with reference to the once-per-revolution pulse, which is generated by a photodetector mounted on the compressor shaft. This helped in tagging the valid data point with the angular position of the rotor. Thus, the data transferred to the computer consisted of three words of 16 bits each. They include the information about the time, N cycles, and reference time.

The velocity measured is realized randomly along the circumferential direction because of the random interception of the probe volume by seed particles. At any instant in time, when the system is ready to accept the data, 1450 data points are transferred into the main core. Before the system is ready to accept another data set, the data contained in the memory are processed. Each processed data point represents the Doppler frequency shift associated with the respective tangential location for a passage. The maximum distribution of the points in a passage is 150. The data pertaining to a selected passage in the rotor are retained, and the remaining data are discarded. If necessary, the data from all of the passages could be combined and averaged as representative data for a passage. During the data acquisition, a graphic terminal is used to generate a graphic display of the data, which is updated after 1450 data points are accepted. Thus, the data is monitored continuously and terminated if necessary. At the end of each run

$$N_J, \quad \sum_{i=1}^{N_J} f_i$$

are stored in the memory. N_J is the total number of measurements at the Jth location in the passage, and f_i is the Doppler frequency shift of the ith measurement at the Jth location. The data reduction and error analysis are very similar to those described in Refs. 5 and 6, therefore, only a brief description is given below.

Error Estimate

Both the axial and tangential velocity components near the tip region of the compressor rotor were measured using the LDV. Measurement of either component was made by rotating the plane of the beam. No attempt was made, however, to measure the radial component.

The error in locating the problem volume is ± 0.025 mm. The error involved in the beamsplitter setting is ± 0.03 deg. Errors induced in measuring the mean flow velocity arise due to 1) fluctuations in the flowfield and random noise due to the photomultiplier tube, 2) statistical or velocity bias, and 3) angle or fringe bias.

The error due to flow fluctuation and random noise from the photomultiplier tube is difficult to estimate. The random noise generated by a photomultiplier tube depends on the background radiation; hence, this noise varies from one measurement to the other. Fluctuation in the flow may be caused by the drift in the rotor speed. In the present case, the drift in the rotor speed is nearly 0.18%. Other primary causes of flow fluctuation are turbulence and the gradient of the velocity at the point of measurement across the rotor passage. The measurement error is a function of the number of samples, and the ratio of standard deviation to the mean velocity. Using the analysis of Ref. 6, the error in the mean flow velocity measurement, for a confidence level of 95%, was estimated to be about 2.5% in the highest turbulence region. The error due to the velocity gradient is assumed to be negligible due to the fact that any spatial variation of the flowfield in a region as small as the probe volume is negligibly small. The error due to the velocity gradient is extremely important in the flowfield associated with normal shock.

The velocity or statistical bias is introduced mainly by the data rate variations. In a flow with uniform seeding, a large number of seed particles intercept the probe volume when the velocity is higher than the mean, and vice versa when the velocity is lower than the mean. A high data rate causes the measured values to be biased toward a higher value than the true mean. An estimate of the error due to statistical bias is about 1%, based on the analyses of Refs. 6 and 8.

An error occurs when the flow is not parallel to the plane containing the laser beams. This error is termed fringe or angle bias.[6] For a single-component system, the probability of making a measurement decreases by 10% when the velocity vector forms an angle of 37 deg with the line perpendicular to the fringe pattern. The factor that controls the fringe bias is the ratio of N/N_{FR}, where N is the minimum number of cycles required by the signal processor and N_{FR} the number of measurable fringes. The fringe bias can be minimized by reducing the ratio N/N_{FR}. The ratio N/N_{FR} can be reduced by either decreasing N or increasing N_{FR}. The former is a function of the processor, whereas the latter depends on the optics. Use of frequency shift is an effective means to minimize the fringe bias. In the present case, the fringe bias is maximum in the end-wall region, and minimized by decreasing N.

The selection of the seed particle for successful LDV measurement depends on many factors. These factors are discussed in detail in Ref. 7.

Experimental Results

Although a large amount of data was acquired during this investigation, only the representative data are given in a compact format in the form of three-dimensional plots. The

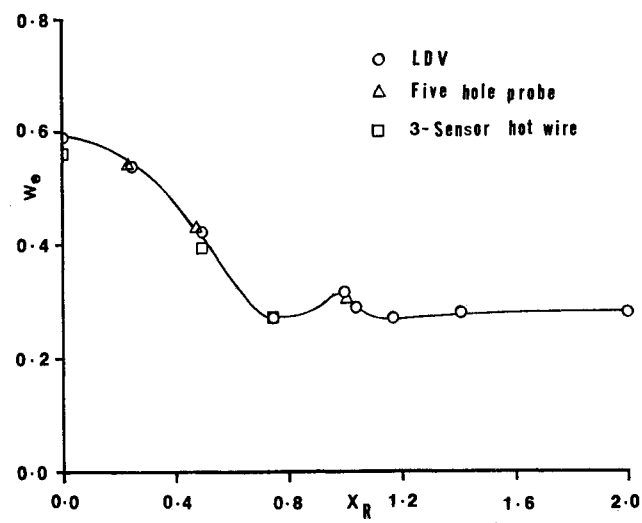

Fig. 3 Comparison of LDV, five-hole probe, and three-sensor hot-wire probe data at $R=0.902$ and $Y=0.5$.

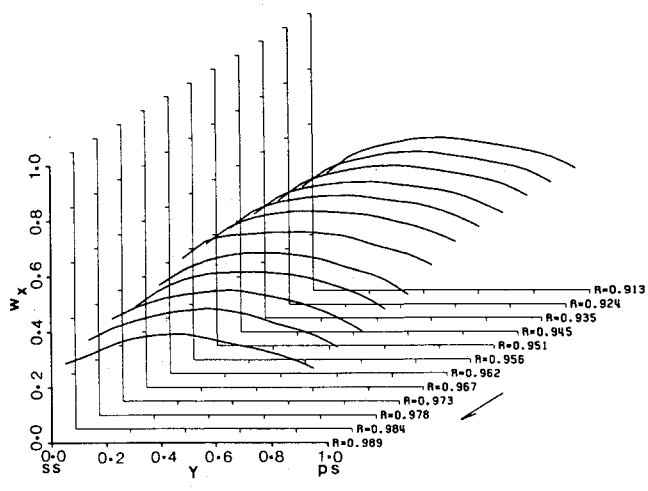

a) $X_R = 0.0$, leading edge.

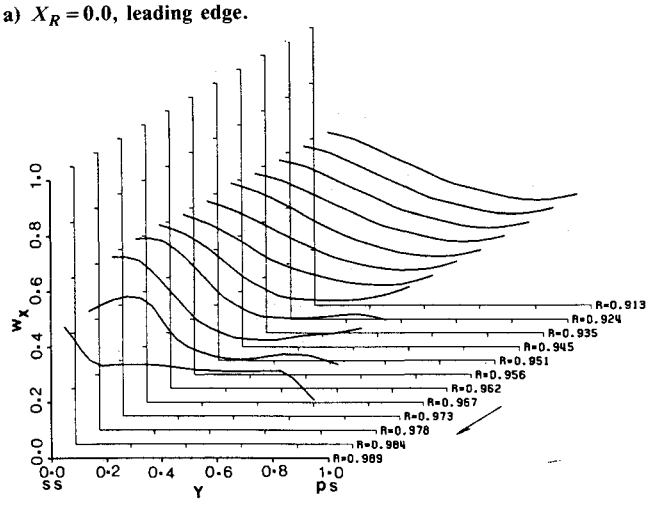

b) $X_R = 0.25$.

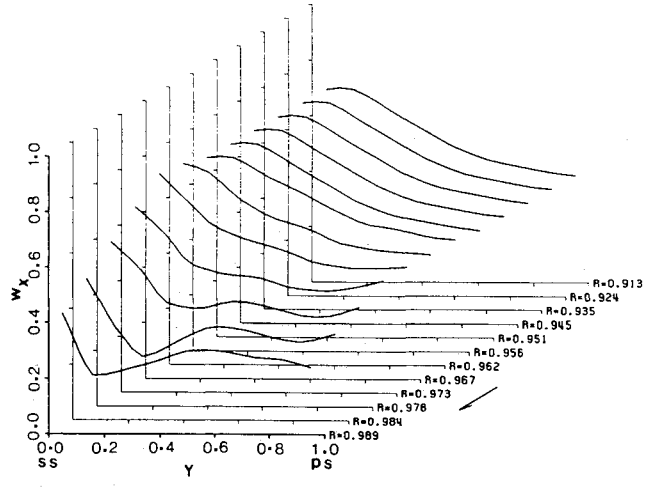

c) $X_R = 0.50$.

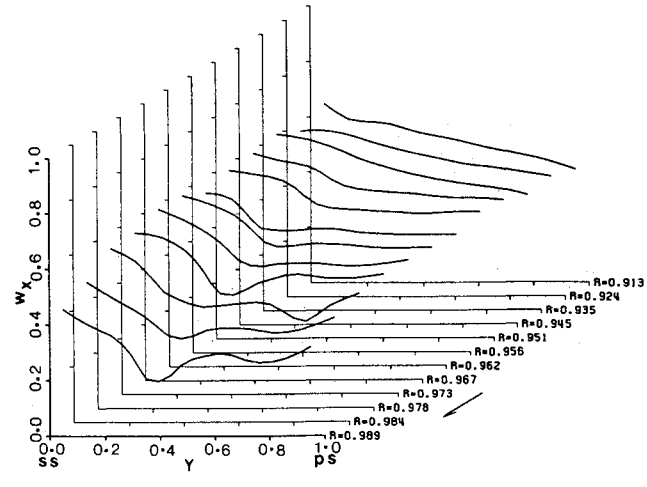

d) $X_R = 0.75$.

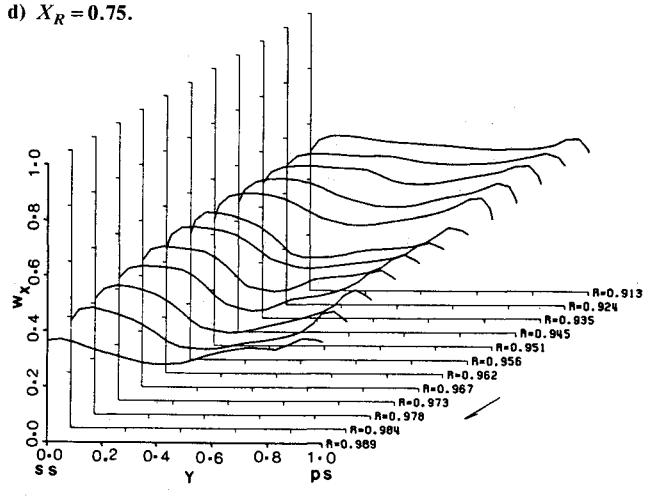

e) $X_R = 1.0$, trailing edge.

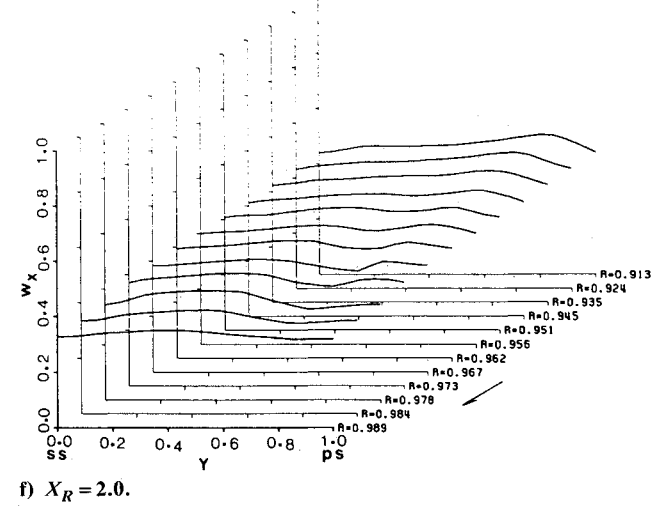

f) $X_R = 2.0$.

Fig. 4 Axial velocity profiles.

complete data set is presented in Ref. 7. As indicated earlier, only the axial and the tangential components of the velocity have been measured and reported in this paper.

In all of these plots, the velocities are normalized by blade tip speed, and PS and SS refer to the pressure surface and suction surface, respectively.

Comparison of the LDV, Three-Sensor Hot-Wire, and Five-Hole Probe Data

In order to validate the LDV measurement, the data were acquired initially at several locations inside the passage where the measurements from the conventional probes (three-sensor hot-wire and five-hole probes) were available.[1] The data from conventional probes may be in error in close proximity to the wall and the blade surfaces. Hence, it is appropriate to compare the LDV data with conventional probe measurements in regions where such aerodynamic interferences are small.

Comparison of the relative tangential velocity at the midpassage and at $R = 0.902$ is shown in Fig. 3. The agreement between the three experimental data sets is good, with the exception of the three-sensor hot-wire data at the leading edge.

The comparisons between the three sets of data at $R = 0.918$ and $X_R = 0.5$ and 1.04 are given in Ref. 9. The

agreement between all three data sets is good in most locations. Discrepancy is observed near the blade surfaces and in the regions where the interaction effects are present. The maximum discrepancy between these measurements is as much as 15% close to the blade location. This discrepancy may have been caused by the probe interference in the cases of the five-hole and three-sensor hot-wire probes.

Axial Velocity Distribution

The variations of the axial velocity across the rotor passage at various axial locations are shown in Figs. 4a-f. The axial velocity distribution across the passage, at the leading edge of the rotor ($X_R = 0$), is shown in Fig. 4a. The variation in axial velocity in the region close to $Y = 0.05$ and 0.95 is substantial, and is mainly caused by the inviscid effects. The axial velocity decreases substantially near the leading-edge region of the suction surface due to large flow turning. The decreases in the axial velocity near the pressure surface is due to flow deceleration in the neighborhood of the stagnation point. This phenomenon results in a substantial defect in the axial velocity near the blade surfaces at the leading edge. The deceleration of the flow in the proximity of the leading edge causes the flow to accelerate away from the surfaces resulting in a peak at the midpassage.

As the flow develops along the rotor passage, the flow in the tip region is affected by the leakage flow from the pressure to the suction side. The effects of leakage flow can be seen in Fig. 4b, which shows the axial velocity variation at the one-quarter-chord location ($X_R = 0.25$). The blade-to-blade variation of the axial velocity shows a small defect from the suction surface to approximately 40% of the passage from $R = 0.989$ to 0.967. The defect decreases toward the lower radii.

At the midchord location ($X_R = 0.5$), the axial velocity distribution (Fig. 4c) exhibits deficiency to nearly half the passage width from the suction surface and from $R = 0.989$ to 0.978. The deficiency in the velocity may be attributed partly to the blade and annulus-wall/boundary-layer interaction, and mainly to the tip leakage flow. The effects of the leakage flow close to the suction surface of the blade tip are evident from the deficiency in velocity observed from $R = 0.962$ to 0.989. In this region, the interaction between the leakage jet and the mean flow manifests as stagnation pressure and total velocity defects. The leakage flow starts to develop at approximately the one-quarter-chord position and grows in strength at the midchord location. Similar evidence was found in Ref. 1. The effect due to the tip leakage is further supported by similar trends in tangential velocity variation presented later. The flow is predominantly inviscid from $R = 0.913$ to 0.962, showing a peak at the suction surface. The velocity defect in the vicinity of the blade surfaces observed at the leading edge has decreased substantially at both the one-quarter-chord and midchord locations.

The flowfield past the three-quarter-chord location ($X_R = 0.75$) (Fig. 4d) is dominated by the mixing of the leakage jet with the main flow. The leakage flow emanating as a jet from the pressure to the suction side tends to blow the suction surface blade boundary layer and suck the blade boundary layer on the pressure side. As a result, the flowfield appears extremely complex (see Fig. 4d). The effects of leakage flow have propagated to full passage width and up to $R = 0.945$. The blade rotation also helps to spread the leakage jet toward the pressure surface. The regions of low axial velocity magnitude now occur farther away from the blade suction surface and the defect is much larger than those observed at the midchord location. This indicates the dominant influence of the leakage flow, and its eventual roll-up and transport toward the midpassage. In the present investigation, the blade boundary layer is not resolved accurately due to the presence of the blade shadow.

At the trailing edge (Fig. 4e), the region bounding the entire passage from the blade tip to $R = 0.935$ has been influenced by the leakage flow, which appears to be diffusing. The blade boundary layer/wake can be seen on both surfaces at this axial location. At about an axial chordlength downstream of the rotor ($X_R = 2.0$), the leakage flow decay (Fig. 4f) is almost complete. The annulus-wall boundary layer is uniform once again and has grown in comparison to that observed at the leading edge.

Relative Tangential Velocity Distribution

The variation of the relative tangential velocity across the rotor blade passage is shown in Figs. 5a-f at various axial locations. The graphs are plotted differently from the axial velocity plots (Fig. 4) to show clearly the leakage flow development.

Figure 5a shows the variation of tangential velocity across the rotor passage at the leading edge ($X_R = 0.0$). The flow is predominantly inviscid, having maximum velocity on the suction surface and minimum velocity on the pressure surface except near the blade tip. An increase in velocity magnitude at the tip region, in the proximity of the pressure surface, is caused by the leading-edge effects of the rotor blade. The probe volume, when traversed from the tip toward the hub, gradually intercepted the leading edge of the rotor. At the tip, the absolute tangential velocity component was measured in the vicinity of the leading edge (away from it); whereas toward the lower radii, the absolute tangential velocity component was measured in the proximity of the blade surface (downstream of the leading edge). This accounts for the difference in the relative tangential velocity component observed near the pressure surface from $R = 0.913$ to 0.989.

At the one-quarter-chord location ($X_R = 0.25$), the blade-to-blade variation of the relative tangential velocity component (Fig. 5b) has a small velocity defect near the suction surface of the blade tip. This defect in velocity clearly indicates the inception of the leakage flow. The leakage jet roll-up near the suction surface causes the velocity defect. Likewise, the leakage flow results in an increase in the relative tangential velocity near the pressure surface.

As the flow develops, the leakage jet spreads; and, aided by blade rotation, tends to move away from the suction surface. The spreading of the leakage jet is clear as can be seen in Fig. 5c, which shows the relative tangential velocity distribution at the midchord. As noted in the axial velocity distribution, the leakage effect is confined to nearly one-half the passage width from the suction surface and from $R = 0.989$ to 0.978. The leakage flow effects are felt to nearly one-quarter of the passage from $R = 0.973$ to 0.951.

The nature of leakage flow and its eventual roll-up to form a vortex or a mixing region is shown in Fig. 6. Due to the blade motion, the leakage jet moves farther away from the suction surface (unlike the leakage jet from a stationary blade). The jet tends to rollup inside the passage to form a vortex. This phenomenon leads to a higher relative tangential velocity (than the design) in the outer radii, and a lower relative tangential velocity (than the design) toward the lower radii. This observation is confirmed by the velocity profiles presented in Figs. 5a-f. The troughs in the relative tangential velocity distribution in the radial direction are similar to that of a vortex. The vortex (indicated by troughs in the distribution) moves away from the suction surfaces as the flow progresses downstream. Thus, the vortex or jet is convected by the main flow. The distribution also shows a trend wherein the vortex strength is augmented by the leakage flow emanating from various chordwise locations.

Figure 5d shows the tangential velocity distribution at the three-quarter-chord location ($X_R = 0.75$). The leakage jet (or vortex) has moved farther away from the suction surface, covering almost the full passage width and nearly 10% of the blade span. The trough-like distribution in the radial direction occurs at approximately the middle of the blade passage.

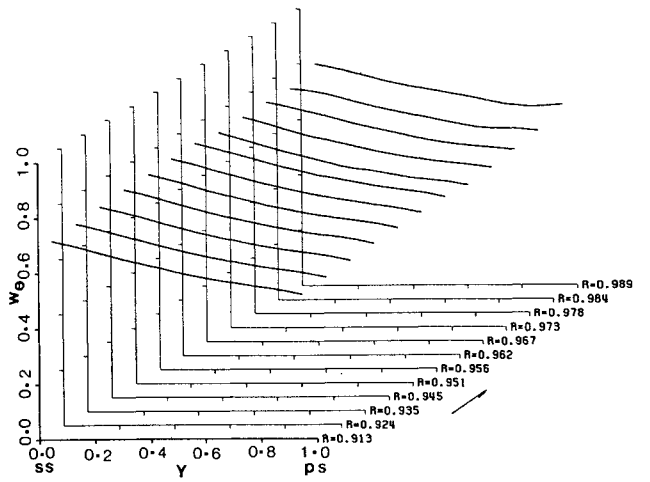

a) $X_R = 0.0$, leading edge.

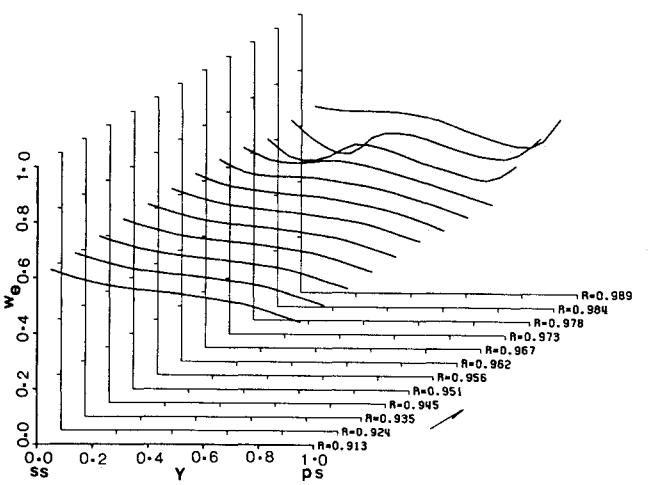

b) $X_R = 0.25$.

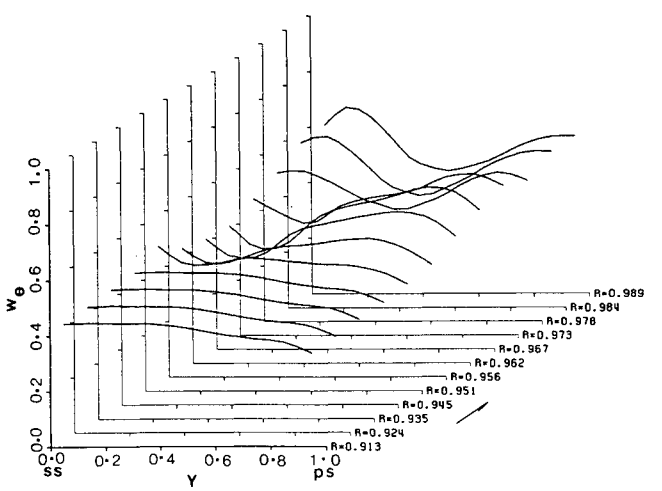

c) $X_R = 0.5$.

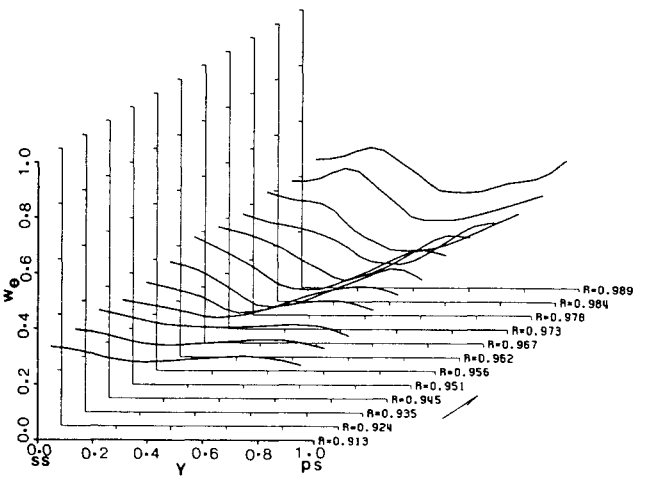

d) $X_R = 0.75$.

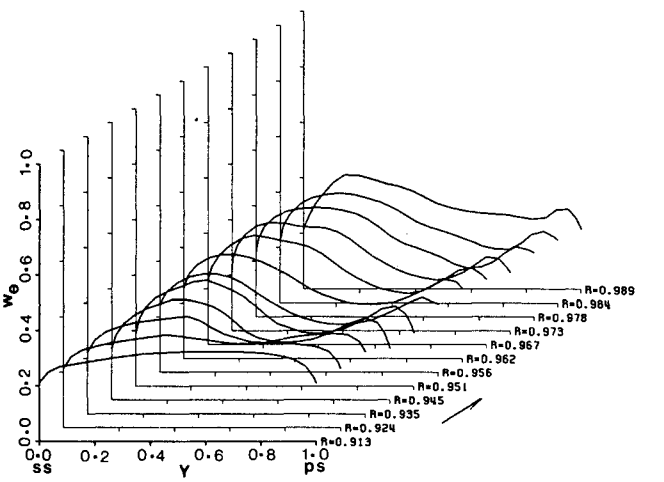

e) $X_R = 1.0$, trailing edge.

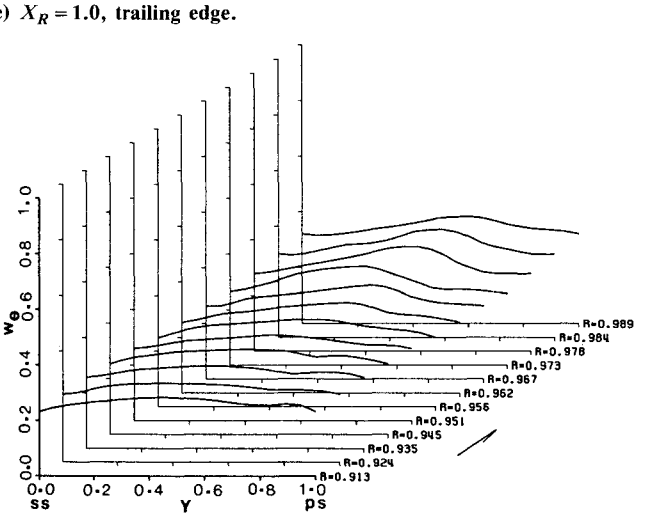

f) $X_R = 2.0$.

Fig. 5 Relative tangential velocity profiles.

The flow downstream (Fig. 5e) is accompanied by spreading of the leakage jet (vortex). As a result, its effect is being felt in the entire passage, and to nearly 12% of the blade span. The strength of the jet (or the vortex) seems to have been augmented by the leakage flow emanating along the entire chordlength. The effects of the leakage jet or vortex persist even up to $X_R = 1.41$, beyond which it is dissipated. The relative tangential velocity profile at one axial chord downstream (Fig. 5f) indicates the complete mixing of the leakage jet or vortex.

Contour Plots of Resultant Velocity

The isocontours of the total velocity ($W_{x\theta} = \sqrt{W_\theta^2 + W_x^2}$) at the axial station $X_R = 0.25$, 0.5, 0.75, and 1.0 are shown in Fig. 7. At the leading edge (not shown in the figure), the main effect is due to the inviscid flow turning and the annulus-wall boundary layer. The leakage flow originated at the quarter-chord location (cf., Figs. 4b and 5b); however, the influence of the leakage flow on the total velocity distribution seems to be insignificant at this location. The distorted contours toward the tip might have been caused by

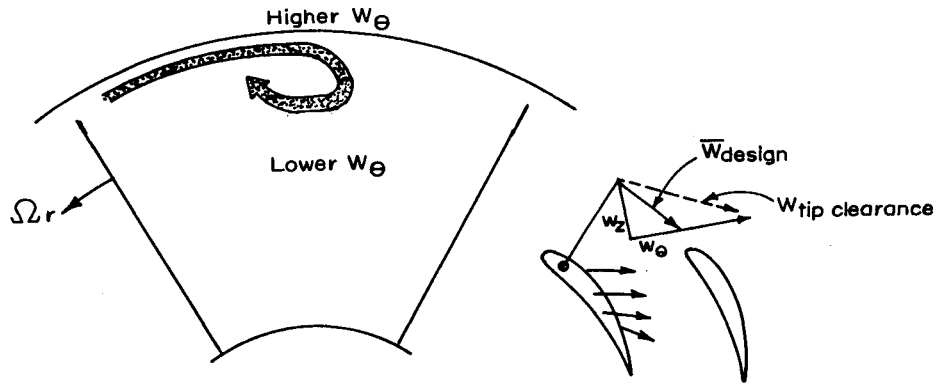

Fig. 6 Nature of leakage flow.

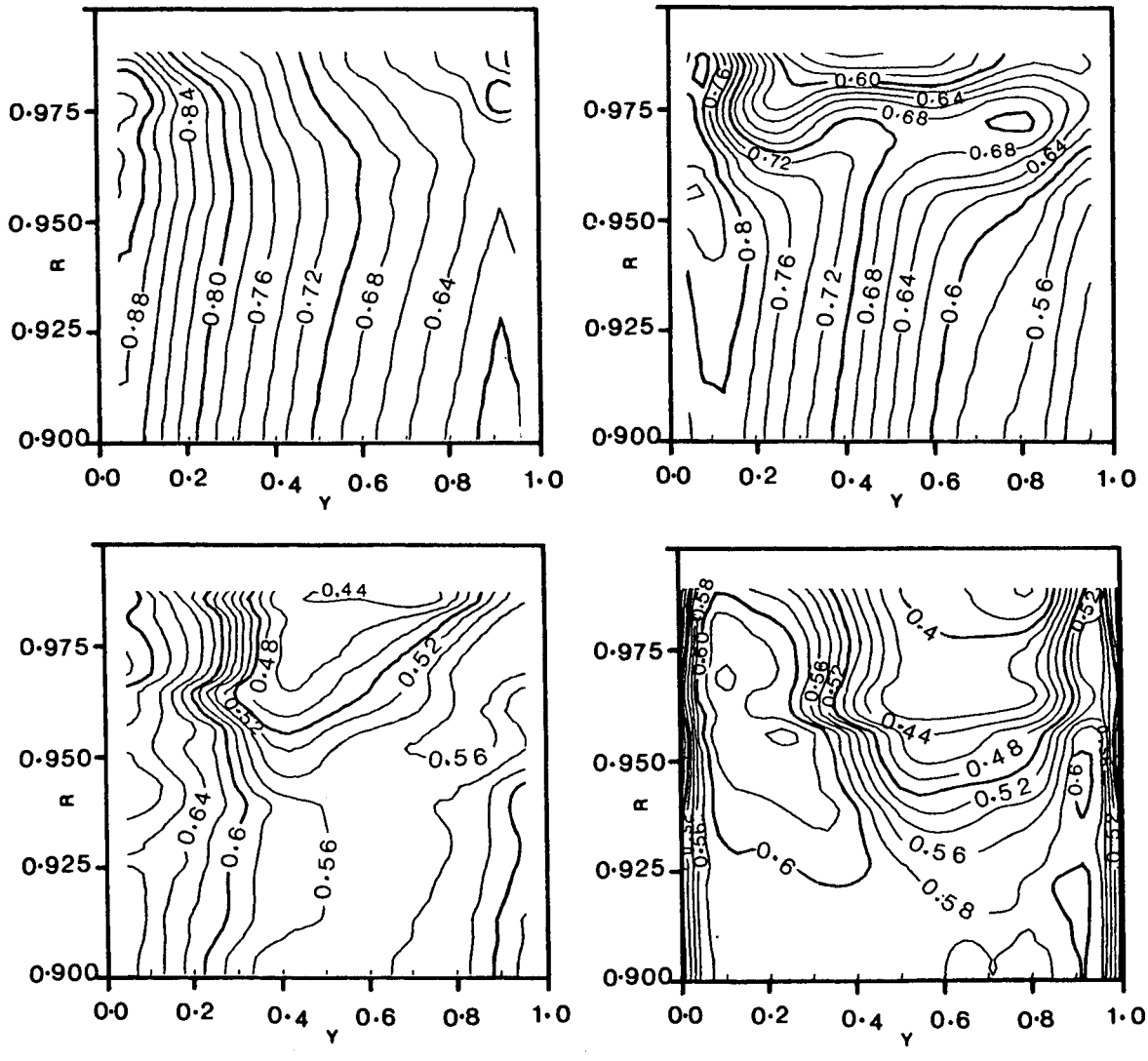

Fig. 7 Isocontours of $W_{\theta x}$ at $X_R = 0.25$, 0.5, 0.75, and 1.0 (the values denote the magnitude of $W_{x\theta}$).

the interaction between the inviscid flow and the annulus-wall boundary layer. A region of the flowfield associated with high acceleration is evident near the suction surface. At midchord, interaction between the leakage flow and the main flow manifests as a stagnation pressure defect reflected in the total velocity isocontours shown in the figure. At the three-quarter-chord location, the influence of the leakage flow is felt below the radial location $R = 0.950$, and a core of total velocity defect is located at approximately $Y = 0.5$. At the trailing edge, the leakage flow has significantly influenced the flowfield in the entire blade passage from the rotor tip to $R = 0.925$.

Conclusions

The LDV data have provided a quantitative understanding of the flow phenomena in the tip region of a compressor rotor. The LDV is found to be an invaluable tool in understanding the flow in the proximity of the leading edge and the tip region of the compressor rotor. The LDV data are validated with earlier measurements based on the rotating five-hole probe and the rotating three-sensor hot-wire probe.

The major conclusions of this paper are:

1) The inception of the leakage jet and its eventual roll-up result in higher and lower relative tangential velocity com-

ponents at higher and lower radii, respectively. This has the effect of underturning of the flow at higher radii and overturning at lower radii. This conclusion is similar to the conclusion drawn from the investigations using a cascade of blades.

2) The leakage jet (vortex) seems to originate at approximately quarter-chord and spreads toward the pressure surface to form a complex mixing region. The region extends to nearly 12% of the blade span at the tip.

3) The spreading of the leakage jet (vortex) is partly due to the diffusive nature of the jet, and is augmented by the blade rotation.

4) The leakage flow is convected downstream and augmented by the leakage flow emanating along the entire chordlength.

Acknowledgments

This work was supported by the National Aeronautics and Space Administration through Grant NSG 3212, with Dr. P. Sockol as the Grant Monitor. The authors wish to thank T.R. Govindan for his help with the installation and shakedown test of the LDV system, and the software development associated with the data processing. The authors also wish to thank Dr. A. J. Strazisar for helpful discussions. Dr. D. Wisler's thorough review and comment on this paper are gratefully acknowledged.

References

[1]Pouagare, M. and Lakshminarayana, B., "Three Dimensional Flow Field Data in a Low Speed Axial Flow Compressor Rotor Passage," to be published as NASA CR, 1986.

[2]Dring, R. P., Josyln, H. D., and Hardin, L. W., "An Investigation of Axial Compressor Rotor Aerodynamics," *Journal of Engineering for Power*, Vol. 104, Oct. 1982, pp. 84-96.

[3]Wisler, D. C. and Mossey, P. W., "Gas Velocity Measurements within a Compressor Rotor Passage Using the Laser Doppler Velocimeter," *Journal of Engineering for Power*, Vol. 95, 1973, pp. 91-96.

[4]Runstadler, P. W. Jr. and Dolan, F. W., "Design, Development, and Test of Laser Velocimeter of High-Speed Turbomachinery," *The Accuracy of Flow Measurements by Laser Doppler Methods, Proceedings of LDA Symposium*, Copenhagen, 1975, pp. 523-552.

[5]Powell, J. A., Strazisar, A. J., and Seasholtz, R. G., "Efficient Laser Anemometer for Intra-Rotor Flow Mapping in a Turbomachinery," *Journal of Engineering for Power*, Vol. 103, 1981, pp. 424-429.

[6]Strazisar, A. J. and Powell, J. A., "Laser Anemometer Measurements in a Transonic Axial Flow Compressor Rotor," *Journal of Engineering for Power*, Vol. 103, 1981, pp. 430-437.

[7]Murthy, K.N.S., "An Experimental Investigation of End-Wall Flow Field in a Compressor Rotor," Ph.D. Thesis, Department of Aerospace Engineering, The Pennsylvania State University, University Park, PA, 1985.

[8]Barnett, D. O. and Bentley, H. T., "Statistical Bias of Individual Realization Laser Velocimeters," *Second International Workshop on Laser Velocimeter*, Vol. 1, edited by H. D. Thompson and W. H. Stevenson, Purdue University, West Lafayette, IN, 1974, pp. 428-444.

[9]Murthy, K.N.S. and Lakshminarayana, B., "Laser Doppler Velocimeter Measurements in the Tip Region of a Compressor Rotor," AIAA Paper 84-1602, 1984.